Territory splitting revisited in prioritized multiobjective optimization

Jean-Antoine Désidéri

Territory splitting revisited in prioritized multiobjective optimization

Jean-Antoine Désidéri

RESEARCH REPORT
N° 9568
January 8, 2025
Project-Team Acumes

ISSN 0249-6399 ISRN INRIA/RR--9568--FR+ENG

Territory splitting revisited in prioritized multiobjective optimization

Jean-Antoine Désidéri*

Project-Team Acumes

Research Report n° 9568 — January 8, 2025 — 24 pages

Abstract: This report is a follow-up on the prioritized optimization method introduced to handle multiobjective optimization problems under constraints in concurrent engineering when the cost functions are differentiable and can be split into two groups: *(i)* the primary cost functions (Group A) that are of preponderant importance and whose optimization is carried out firstly yielding a Primary Pareto Front (PPF); *(ii)* the secondary cost functions (Group B) to be reduced in a second phase of optimization initiated from a point of the Primary Pareto Set in a way that should least degrade the Pareto-stationarity condition. This second phase implies two virtual players whose strategies are defined in two supplementary subspaces U and V of the design space and yields a continuum of Nash equilibria. We presently show that the orthogonal decomposition permitting to define U and V and establish convergence is solely subject to the condition that U should be tangent to the local constraint surfaces. Generalizing the original method, several such territory splittings are proposed, compared and tested over a sizing problem in structural mechanics. Besides, a simple procedure to rescale the cost functions is shown to yield a better-conditioned optimization system.

Key-words: differentiable multiobjective optimization, criterion prioritization, Nash game

* Inria Research Director, emeritus, Acumes Project Team

RESEARCH CENTRE
Centre Inria d'Université Côte d'Azur
2004 route des Lucioles - BP 93
06902 Sophia Antipolis Cedex

Partage de territoire revisité en optimisation multiobjectif hiérarchisée

Résumé : Ce rapport fait suite à la méthode d'optimisation priorisée introduite pour traiter les problèmes d'optimisation multiobjectif sous contraintes en ingénierie concourante lorsque les fonctions de coût sont différentiables et peuvent être séparées en deux groupes : *(i)* les fonctions de coût principales (Groupe A) qui sont d'importance prépondérante et dont l'optimisation est réalisée en premier lieu en produisant un Front de Pareto Primaire (FPP) ; *(ii)* les fonctions de coût secondaires (Groupe B) qui doivent être réduites dans une seconde phase d'optimisation initiée à partir d'un point Pareto-optimal vis-à-vis des seules fonctions coûts primaires de manière à dégrader le moins possible la condition de Pareto-stationnarité. Cette seconde phase implique deux joueurs virtuels dont les stratégies sont définies dans deux sous-espaces supplémentaires U et V de l'espace de conception et produit un continuum d'équilibres de Nash. Nous montrons ici que la décomposition orthogonale permettant de définir les sous-espaces U et V et d'établir la convergence est uniquement soumise à la condition que U soit tangent aux surfaces de contraintes locales. Généralisant la méthode originelle, plusieurs partages de territoire de ce type sont proposés, comparés et testés sur un problème de dimensionnement en analyse structurelle. En outre, on montre que l'utilisation d'une procédure simple de redimensionnement des fonctions de coût améliore le conditionnement du système d'optimisation.

Mots-clés : optimisation multiobjectif différentiable, hiérachisation des critères, jeu de Nash

Contents

1 Introduction

In a numerical approach to a problem of concurrent engineering, the practitioner typically defines a set of cost functions to be minimized, say Group A, and a practical set of variables, as well as constraint functions, and makes use of an efficient multiobjective optimization method to identify partially or completely the Pareto set. Several techniques can be employed for this purpose, e.g.: the genetic algorithm NSGA-II [1], Bayesian Optimization [10], or a gradient-based method such as [3]. However once this task is accomplished, the designer still has to use a rational argument to finalize the selection among the Pareto-optimal solutions. One standard way is to define an additional cost function, forming Group B, here as a singleton, evaluate the new cost function over the numerical Pareto set and select the point where it is minimal. In this results the most elementary form, simplistic in our stand, of "prioritized optimization" in which Group A, primary, and Group B, secondary, are optimized sequentially. For example, in the optimal sizing of a structural element under loads, the designer may finalize the selection using a minimum-energy-based criterion.

In order to generalize one such prioritized approach, one may consider a Group B that includes several secondary cost functions . If these are independent, the design cannot be sought to respect strictly the Pareto-optimality condition of Group A. The condition ought to be relaxed. In our approach, it is replaced by a notion of neighborhood, in a sense defined subsequently.

For example, in the preliminary design of a civil aircraft, a shape optimization may be conducted with respect to classical aerodynamic performance criteria. In this exercise, the practitioner would very naturally first consider the concurrency between a drag reduction in cruise conditions (to maximize potential range, or minimize embarked fuel and environmental impact) against a lift maximization in conditions representative of the ascent phase (for purpose of safety). However to validate the concept, the aerodynamic performance should also be assessed with respect to other important mission performance measures such as landing speed, take-off distance, pitching moment range, etc. In an advanced optimum-shape design these other measures may also take part in the optimization, through a secondary set of criteria.

Considering the Pareto front identification method for Group A, note that it implies a computational effort that may increase rapidly with the number of objective functions. This increase may be severe when the introduction of new criteria requires a specific functional evaluation by new differential equations, which is typical of a multidisciplinary context, or due to the increase in the algorithmic complexity of the numerical method itself, as it is the case for NSGA-II. The prioritized optimization approach which handles the cost functions progressively is advocated here to attenuate this difficulty.

In this perspective, a prioritized multiobjective numerical optimization method was devised for concurrent engineering. It was theoretically proved convergent, and numerically experimented, mostly in [2] [4] [5] and [9]. The optimization is subject to K usually nonlinear and functional constraints ($K \geq 1$), all of equality type, possibly after the introduction of slack variables for the treatment of bound or interval constraints. Each physical optimization variable is subject to specified bounds and these are handled by transformation of the admissible domain into the hypercube $[-1, 1]^n$, where n is the number of optimization variables in the initial physical formulation. Assuming that all constraints are of equality type, possibly via the introduction of s slack variables, the total number of working optimization variables is

$$N = n + s. \tag{1}$$

The slack variables are usually evaluated without additional instantiation of the possibly-costly physical simulation code. The present numerical method for prioritized optimization develops in three stages.

Stage 1: This stage is the determination of at least one Pareto-optimal point $\mathbf{x}_A^\star$ w.r.t. the sole primary objective functions (Group A) under constraints. Most often the entire Primary Pareto Front (PPF) is identified numerically and $\mathbf{x}_A^\star$ is selected in it.

Stage 2: After the election of the point $\mathbf{x}_A^\star$, local meta-models for all objective and constraint function(al)s need be elaborated. If Bayesian optimization is used at Stage 1, some meta-models do already exist and Stage 2 may be skipped or simply completed. Otherwise, a Design of Experiment (DoE) is necessary for the purpose of constructing local quadratic models about $\mathbf{x}_A^\star$. All functions of interest are evaluated over a geometrical database. One way to define the geometrical database has been described in details in [9] and it is here slightly modified to better handle the case of a point $\mathbf{x}_A^\star$ on a boundary of the admissible domain, or very close to it (see Appendix **??** The DoE is conducted in R^n since the physical functions do not depend on the slack variables. Then the database is extended to R^N at usually negligible cost by evaluating the constraint violations at the datapoints via formulas. In total the DoE involves $16n(n-1)+2n+1$ functional evaluations.

Stage 3: The third and final stage is the calculation of a continuum of Nash equilibria forming a path originating from $\mathbf{x}_A^\star$ parameterized by a variable ε varying from 0 to a limit of convexity $\varepsilon_{\max} \leq 1$.

The development of Stage 3 relies on a special split of variables, here referred to as "territory splitting". In former publications this splitting was defined in a unique way relying only on the cost functions of Group A and the constraint functions. The aim of this report is to propose possible alternative splittings to include a partial dependency on Group B. This is accomplished in Section **??** after some generalities are first established.

2 Hessians and steering functions

Given the point $\mathbf{x}_A^\star$, one first identifies for each group the convex combination of the group cost functions for which the corresponding combination of local gradients has minimum Euclidean norm. The coefficients of the corresponding combination serve to define the group steering function.

For Group A, the projected gradients are used, and the combined function is locally minimum by hypothesis of Pareto optimality, as a special case of (14) for $\varepsilon = 0$. But in practice, due to numerical errors, the Hessian or the Lagrangian Hessian may have one or several negative eigenvalues of small absolute values. In such a case, the combination is given a "convexity fix" indicated by the superscript $^+$. The fix consists in adding the term $c\left\|\mathbf{x}-\mathbf{x}_A^\star\right\|^2/2$, for an appropriate small coefficient c, to the identified combination of cost functions yielding the locally-convex steering function f_A^+ and its strictly positive-definite Hessian

$$\mathbf{H}_A^+ = \left(f_A^+\right)''(\mathbf{x}_A^\star). \tag{2}$$

For Group B, a similar construction is developed using projected gradients of the secondary cost functions and permitting to give a *preliminary definition of the secondary steering function* f_B and to calculate the following local Hessian

$$\mathbf{H}_B = f_B''(\mathbf{x}_A^\star). \tag{3}$$

No convexity fix is applied to the steering function f_B, since only a reduction of this function is envisaged without a complete minimization.

3 A general class of orthogonal decompositions

The primary optimization problem, that is the minimization of the cost functions of Group A, is subject to K constraints. These are all assumed to be of equality type, possibly after some transformation, and active at the starting point $\mathbf{x}_A^\star$:

$$c_k^\star = c_k(\mathbf{x}_A^\star) = 0 \quad (k = 1, \ldots, K). \tag{4}$$

The QR-algorithm is applied to the $N \times K$ matrix of local gradients $\{\nabla c_k^\star\}$ $(1 \le k \le K)$

$$\nabla \mathbf{c}^\star = \Big([\nabla c_1^*][\nabla c_2^*] \cdots [\nabla c_K^*] \Big) = \mathbf{QR} \tag{5}$$

in which $\nabla c_k^\star = \nabla c_k(\mathbf{x}_A^\star)$ and the notation [.] applied to a vector stands for the column-vector of its components in the canonical basis. The column vectors of matrix $\mathbf{Q}$, say $\{q^k\}$, form an orthogonal basis generating the K-dimensional span of the constraint gradients, i.e. the linear subspace orthogonal to all local constraint (hyper-)surfaces. Then the projection matrix $\mathbf{P}$ onto the K-dimensional tangent subspace is given by

$$\mathbf{P} = \mathbf{I} - \sum_{k=1}^{K} [q^k]\,[q^k]^t. \tag{6}$$

By assumption $\dim \mathrm{Ker}\,\mathbf{P} = K$.

Consider an orthogonal decomposition of the working space R^N into the supplementary subspaces U and V:

$$\mathsf{R}^N = U \oplus V, \quad U \perp V. \tag{7}$$

Assume that U contains $\mathrm{Ker}\,\mathbf{P}$, and that $p = \dim V \le N - K$, and usually $1 \le p < N - K$.

Let $\mathbf{\Omega}$ be an orthogonal matrix ($\mathbf{\Omega}^t\mathbf{\Omega} = \mathbf{I}_N$), whose first K column-vectors form a basis of $\mathrm{Ker}\,\mathbf{P}$. Let $\mathbf{\Omega_u}$ be the left $N \times (N-p)$ block of matrix $\mathbf{\Omega}$, and $\mathbf{\Omega_v}$ the $N \times p$ right block. These blocks are of full rank.

Define the following change of variables

$$\mathbf{x} = \mathbf{x}_A^\star + \mathbf{\Omega_u}\mathbf{u} + \mathbf{\Omega_v}\mathbf{v} = \mathbf{X}(\mathbf{u}, \mathbf{v}) \tag{8}$$

in which $\mathbf{u} \in \mathsf{R}^{N-p}$ and $\mathbf{v} \in \mathsf{R}^p$.

4 Nash game formulation

For ε gradually increasing from 0 to at most 1, one defines the auxiliary function

$$f_{AB} = (1-\varepsilon) f_A^+ + \varepsilon f_B \tag{9}$$

and consider the following Nash game:

$$\text{(A)} \begin{cases} \min_{\mathbf{u} \in \mathsf{R}^{N-p}} f_A^+\big(\mathbf{X}(\mathbf{u}, \mathbf{v})\big) \\ \text{s. t. } \mathbf{c}\big(\mathbf{X}(\mathbf{u}, \mathbf{v})\big) = 0 \end{cases} \quad \text{concurrently with} \quad \text{(B)} \begin{cases} \min_{\mathbf{v} \in \mathsf{R}^{p}} f_{AB}\big(\mathbf{X}(\mathbf{u}, \mathbf{v})\big) \\ \text{s. t. no constraints} \end{cases} . \tag{10}$$

4.1 Initial Nash equilibrium

For $\varepsilon = 0$, $f_{AB} = f_A^+$, simply denoted f below. The following question is raised: is $(\mathbf{u}, \mathbf{v}) = (0, 0) \in \mathsf{R}^{N-p} \times \mathsf{R}^p$ an equilibrium of the above Nash-game formulation? Equivalently, the question is split into two independent questions:

- For $\mathbf{v} = 0 \in \mathsf{R}^p$, does $\mathbf{u} = 0 \in \mathsf{R}^{N-p}$ solve

$$\text{(A)} \begin{cases} \min_{\mathbf{u} \in \mathsf{R}^{N-p}} f\big(\mathbf{X}(\mathbf{u}, 0)\big) \\ \text{s. t. } \mathbf{c}\big(\mathbf{X}(\mathbf{u}, 0)\big) = 0 \end{cases} \quad ? \tag{11}$$

- For $\mathbf{u} = 0 \in \mathsf{R}^{N-p}$, does $\mathbf{v} = 0 \in \mathsf{R}^p$ solve

$$\text{(B)} \begin{cases} \min_{\mathbf{v} \in \mathsf{R}^{p}} f\big(\mathbf{X}(0, \mathbf{v})\big) \\ \text{s. t. no constraints} \end{cases} \quad ? \tag{12}$$

Concerning above Problem (A), the answer is evidently yes since by virtue of the Pareto-optimality of $\mathbf{x}_A^\star$ w.r.t. Group A, this point is a local minimum of f under constraints in the entire working space R^N. Problem (A) only differs from the original primary optimization problem by the restriction of the admissible set. However the restriction preserves the local minimum point $\mathbf{x}_A^\star$ achieved for $\mathbf{u} = 0$.

Concerning above Problem (B), first observe that the Pareto stationarity of f at $\mathbf{x}_A^\star$ requires that the Lagrangian of f be stationary, and this implies that ∇f lies in the span of the constraint gradients. This span, that is $\mathbf{Ker}\,\mathbf{P}$, is contained in subspace U. Hence $\nabla f \in U \perp V$. But for $\mathbf{u} = 0$, the variation $\delta\mathbf{x} = \mathbf{\Omega_v v} \in V$; hence $\delta\mathbf{x} \perp \nabla f$, and the corresponding directional derivative is equal to 0. This establishes the required stationarity property. Hence, $\mathbf{v} = 0$ is indeed a solution to Problem B.

In conclusion, $(\mathbf{u}, \mathbf{v}) = (0, 0) \in \mathsf{R}^{N-p} \times \mathsf{R}^p$ is indeed an equilibrium of the above Nash-game formulation for $\varepsilon = 0$. □

4.2 Subsequent Nash equilibria

For $\varepsilon > 0$, a theorem by Nash permits to guarantee the existence of the equilibrium provided the strategies are compact. This condition is easily satisfied by submitting bounds on $\mathbf{u}$ and $\mathbf{v}$, which is not really restrictive in the neighborhood of the starting point $(\mathbf{u}, \mathbf{v}) = (0, 0)$. Hence the Nash equilibrium exists for sufficiently small ε. □

The construction is such that the Nash equilibrium point $\overline{\mathbf{x}}_\varepsilon$ exists for all sufficiently small ε forming a continuum that is such that:
At the starting point $\mathbf{x}_A^\star$:

1. At $\varepsilon = 0$, $\overline{\mathbf{x}}_0 = \mathbf{x}_A^\star$ ("compatibilty") and the Pareto-stationarity condition writes:

$$\sum_{j=1}^{m} \alpha_j^\star \frac{\mathbf{P}\nabla f_j}{f_j^\star}(\overline{\mathbf{x}}_0) = 0 \tag{13}$$

   where $\mathbf{P}$ is the matrix associated with the projection onto the constraint surfaces.

Along the continuum, for $\varepsilon > 0$:

2. the Pareto stationarity condition of the primary cost functions is only degraded by a term $O(\varepsilon^2)$:

$$\sum_{j=1}^{m} \alpha_j^\star \frac{\mathbf{P}\nabla f_j}{f_j^\star}(\overline{\mathbf{x}}_\varepsilon) = O(\varepsilon^2); \tag{14}$$

3. the secondary cost functions are reduced linearly in ε:

$$\phi_j(\varepsilon) = \frac{f_j(\overline{\mathbf{x}}_\varepsilon)}{f_j^\star} = 1 - \sigma_B\varepsilon + O(\varepsilon^2) \tag{15}$$

   where $\sigma_B = \|\omega_B\|^2 \geq 0$.

(See [5] for a formal presentation and proofs.)

As a result, the graphs of the steering functions in terms of ε diverge, and draw a funnel-type shape, as depicted in Figure 1. In Figure 2, the continuum of Nash equilibria originating from $\mathbf{x}_A^\star$ is represented in the coordinate system of the primary cost functions, assumed to be 2 in number, $\{f_1, f_2\}$, for the purpose of the sketch. The path, in green, is tangent to the hypothetical Primary Pareto Front, in red, illustrating the fact that the deviation from Pareto stationarity is of second order in terms of the curvilinear abscissa.

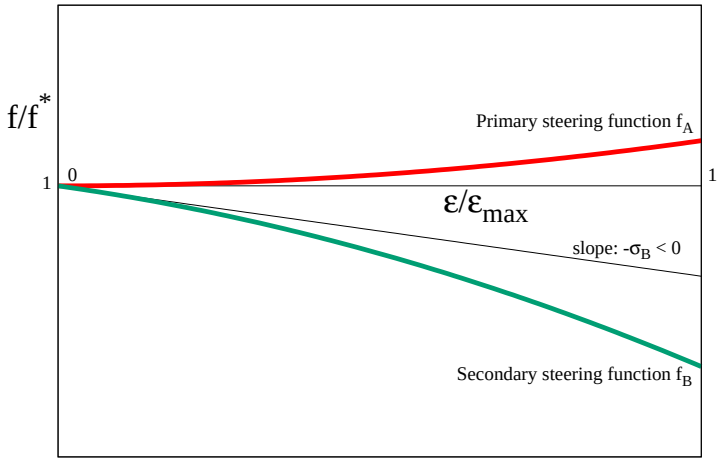

Figure 1: Skematic funnel shape bounded by the two steering functions as ε varies

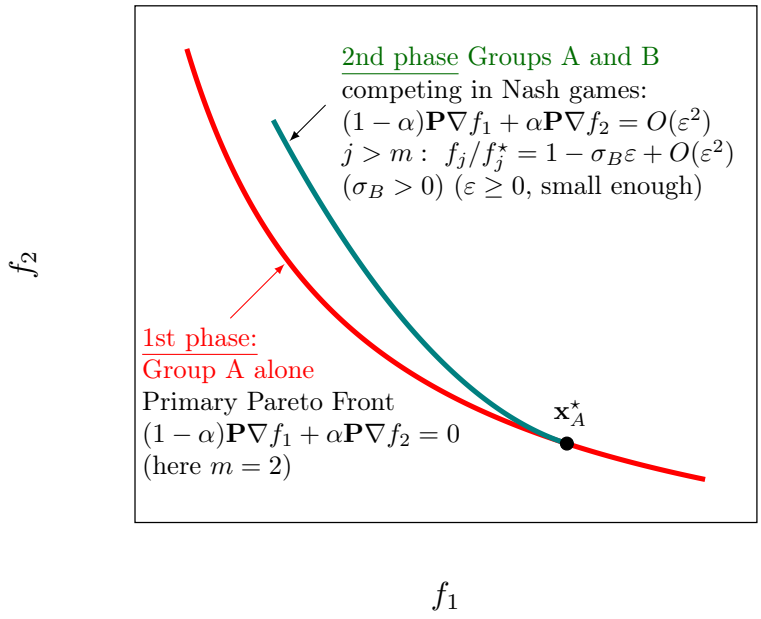

Figure 2: Representation in the space of primary cost functions of the continuum of Nash equilibria (in green) initiated from a point $\mathbf{x}_A^\star$ of the Primary Pareto Front (in red)

5 Original splitting, a test-case, rescaling

5.1 Splitting definition

Our original split is designated by "Split 0" in what follows. It is obtained by letting the matrix $\mathbf{\Omega}$ to be the orthogonal matrix associated with the diagonalization of matrix $\mathbf{H}'_A$, where

$$\mathbf{H}^\star_A = f''_A(\mathbf{x}^\star_A), \quad (\mathbf{H}^\star_A)^+ = \mathbf{H}^\star_A + c\mathbf{I}, \quad \mathbf{H}'_A = \mathbf{P}\,(\mathbf{H}^\star_A)^+\,\mathbf{P} = \mathbf{\Omega}\mathcal{H}\mathbf{\Omega}^t$$

where c, if nonzero, is a small and strictly-positive number introduced to ensure definite-positiveness of the numerical analog of matrix $(\mathbf{H}^\star_A)^+$. In this way, the Taylor's series expansion in ε of $f^+_A(\mathbf{x})$ about $\mathbf{x}^\star_A$ for a $\delta\mathbf{x} = \varepsilon\mathbf{P}\mathbf{w}$ ($\mathbf{w}$: unit vector) in the subspace locally tangent to the constraints writes:

$$f^+_A(\mathbf{x}^\star_A + \varepsilon\mathbf{P}\mathbf{w}) = 1 + \frac{\varepsilon^2}{2}\mathbf{w}^t\mathbf{H}'_A\mathbf{w} + O(\varepsilon^3)$$

since $\mathbf{P}\nabla f^{+,\star}_A = 0$ (Pareto-stationarity). Hence the eigenvectors of $\mathbf{H}'_A$ indicate priviledged directions to maintain the steering function close to Pareto- stationarity. Thus, this splitting strengthens the priorization of Group A, and has been successfully used in several engineering applications:

- Multiobjective design of a SuperSonic-Business Jet (SSBJ) for flight mission optimization. Primary objectives of Nash games: minimization of embarked fuel and maximization of range, subject to upper bound on take-off distance; secondary objective: landing speed reduction [6].
- Optimum sizing of an aluminum sandwich panel. Primary objectives of Nash games: mass minimization and maximization of critical flexural forces, subject to lower bound on thickness; secondary objectives: minimization of deflection and core energy absorption of panel under blast [7].
- Multiobjective design of an Airbus A320-type aircraft for flight mission optimization. Primary objectives of Nash games: minimization of embarked fuel and operational empty weight; secondary objectives: minimization of ascent to cruise altitude duration [8].

Remark 1
This method was observed by numerical experiment to be far more efficient than the more elementary form of prioritized optimization considered firstly in the Introduction in which an element of the Primary Pareto Set (PPS) is chosen simply after the evaluation of a criterion over the PPS, particularly in Test Case TC4 in [7].

5.2 Initial test-case

We consider again the optimum sizing of an aluminum sandwich panel using the same set of 5 variables ($N = 5$) as in [7]: 3 thicknesses, a shape ratio, and a slack variable to enforce a unique constraint, enforcing an upper bound on the total thickness. The point $\mathbf{x}_A^\star$ in the Primary Pareto Set chosen to initiate the continuum of Nash equilibrium is the following:

$$\mathbf{x}_A^\star = (-1.5629544943845421, -1.2000870006928384, -0.83094529619039448, 1.0769290088008954, 0.34345599756029616) \tag{16}$$

Recall that we had introduced several physical cost functions; in particular:

- ϕ_m, proportional to the element mass;
- ϕ_1 and ϕ_2, inversely proportional to the 1st and 2nd critical flexural forces;
- ϕ_w, the deflection at the center of the panel caused by a blast.

In this new test-case, the cost function in the numerical optimization process are chosen to be as follows:

- Primary cost functions: $f_1 = \phi_m$, $f_2 = \phi_1$ ($m = 2$);
- Secondary cost functions: $f_3 = \phi_w$, $f_4 = \phi_2$ ($M = 4$, in total).

The subspace V was chosen to be of dimension $p = 2$ in all the following experiments.

In this setting, Figure 3 provides the main results of the Nash games using the original splitting.

Figure 3a indicates the variation with $\varepsilon/\varepsilon_{\max}$ of the two steering functions in black (solid line for Group A, hatched line for Group B), and the 4 cost functions, each one being normalized by its initial value. The figure evidently confirms the funnel-shape pattern of the representation as anticipated by theory. The primary steering function is initially tangent to the horizontal axis and it points upward, while the secondary steering function points downward; its initial tangent has a small strictly-negative slope ($-\sigma_B = -||\omega_B||^2$). The primary cost functions are plotted in red (mass) and orange (inverse 1st critical flexural force). Mass (in red) increases gradually until the very end of the plot when convexity is insufficient and the calculation blows up. The inverse 1st flexural force (in orange) is almost constant throughout until the sudden drop down. The two secondary cost function (in blue and green) decrease smoothly, and are initially tangent to the secondary steering function as they should be.

Figure 3b provides the variation with $\varepsilon/\varepsilon_{\max}$ of the different variables $\{x_i\}$. Clearly the core thickness x_3 is the most influential variable.

Figure 3c demonstrates that the bound constraint on total thickness is rigorously enforced.

In total, the figure illustrates very well the known theoretical results.

(a) functions $\{f_j\}$

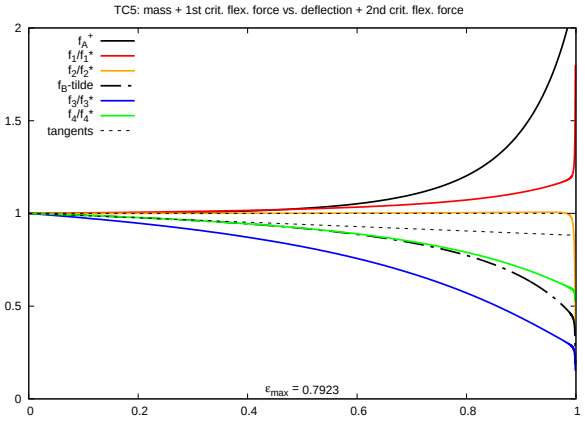

(b) variables x_i

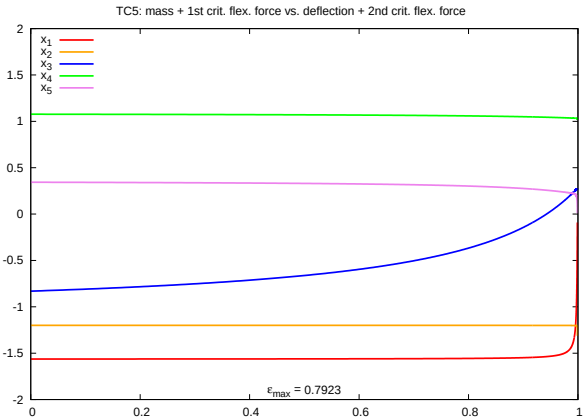

(c) constraint c_1

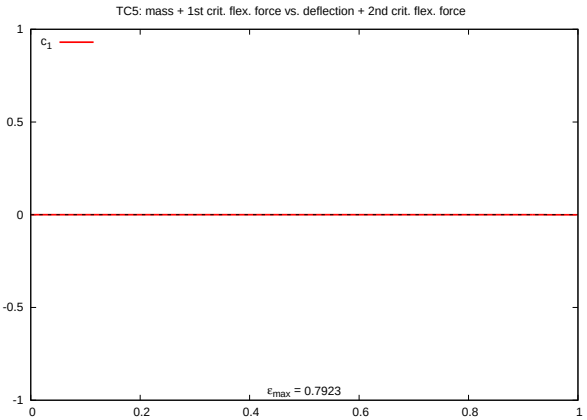

Figure 3: Standard calculation using the original definition of cost functions and splitting

5.3 Rescaling

The above test-case was solved again using a modified, but equivalent, definition of the cost functions. Each cost function $f_j(\mathbf{x})$ was replaced by the following

$$\tilde{f}_j(\mathbf{x}) = \exp\left(\frac{f_j(\mathbf{x}) - f_j^\star}{\|\nabla f_j^\star\|}\right) \tag{17}$$

so that $f_j(\mathbf{x})$ and $\tilde{f}_j(\mathbf{x})$ vary in the same sense; additionally

$$\forall j = 1, \ldots, m: \quad \tilde{f}_j^\star = 1, \quad \nabla\tilde{f}_j^\star = \frac{\nabla f_j^\star}{\|\nabla f_j^\star\|}, \quad \left\|\nabla\tilde{f}_j^\star\right\| = 1. \tag{18}$$

Firstly, let us question how does the Primary Pareto Set evolve in this change of functions. In particular, recall that the expression of the Pareto-stationarity of $\mathbf{x}_A^\star$ in terms of the original cost functions is given in (14). This expression becomes:

$$\sum_{j=1}^{m} \alpha_j \frac{\mathbf{P}\nabla\tilde{f}_j^\star \|\nabla f_j^\star\|}{f_j^\star} = 0. \tag{19}$$

Hence, by letting

$$\tilde{\alpha}_j = \frac{\alpha_j \frac{\|\nabla f_j^\star\|}{f_j^\star}}{\sum_{k=1}^{m} \alpha_k \frac{\|\nabla f_k^\star\|}{f_k^\star}} \tag{20}$$

we get:

$$\sum_{j=1}^{m} \tilde{\alpha}_j \mathbf{P}\nabla\tilde{f}_j^\star = 0 \tag{21}$$

in which the coefficients $\{\tilde{\alpha}_j\}$ are positive and sum up to 1. Lastly, observe that the rescaling has not modified the constraint functions $\{c_k(\mathbf{x})\}$, which leaves the projection matrix $\mathbf{P}$ of (6) unchanged. In conclusion, (21) is the expression of the Pareto-stationarity under constraints of $\mathbf{x}_A^\star$ in the new setting: the Pareto set is unchanged (as expected).

This rescaling is expected to equilibrate the weights between the different cost functions in each group. In particular, when Group A or Group B is composed of two cost functions, as it is the case in our experiment for both groups, the coefficients of the convex combination that define the corresponding steering function are close to $\frac{1}{2}$. To implement this rescaling, the gradient norms were computed by central differencing at $\mathbf{x}_A^\star$.

The results of computing the continuum of Nash equilibria in this new setting are depicted in Figure 4.

Figure 4a demonstrates again the funnel-shape pattern of the cost function plot, perhaps more distinctly since the trend of $\tilde{f}_2$ to decrease is perhaps somewhat more visible. This is confirmed by Figure 4b where the same data are expressed in terms of the original cost functions, $\{f_j\}$, where red and orange curves are closer to be symmetrical w.r.t. the horizontal axis, indicating a closer vicinity with the PPF. Unfortunately, this better behavior of the primary cost functions is achieved at the cost of a reduction of the secondary cost functions that is somewhat inferior to the result of the original formulation, at equal mass increase, as indicated at the same scale in Figure 4c. Hence the preferred formulation remains the practitioner's choice.

(a) rescaled functions $\{\tilde{f}_j\}$ cut at $\tilde{f}_1 = 1.25$

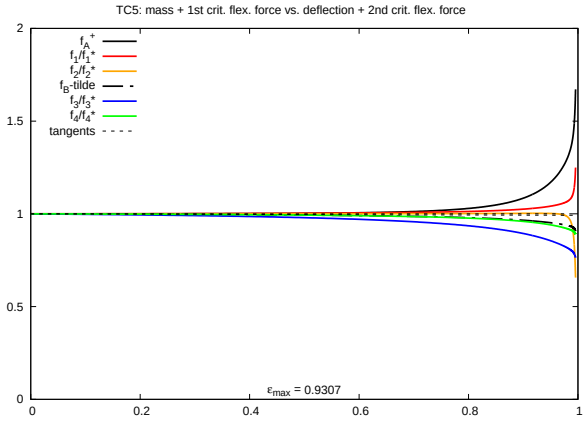

(b) corresponding original functions $\{f_j\}$ at equal cut

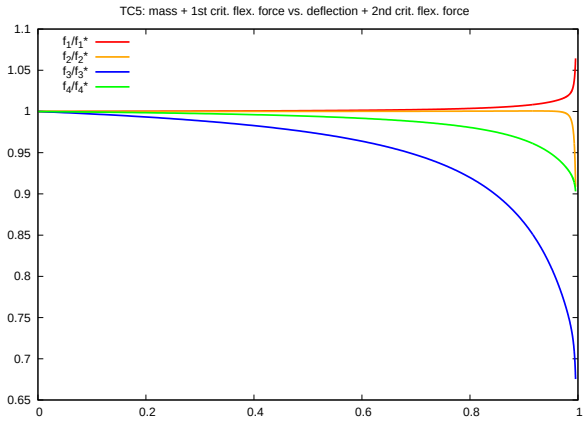

(c) original functions $\{f_j\}$ of Figure 3(a) cut at equal mass increase

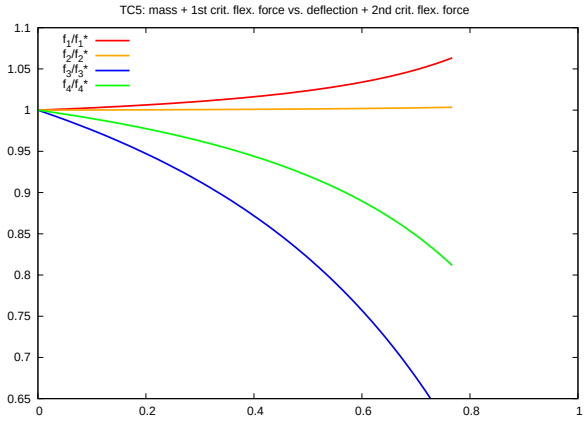

Figure 4: Effect of rescaling functions

6 Territory splitting variants

6.1 Definition

We emphasize that the convergence proof made in Section 4 relied solely on the hypothesis that the orthogonal decomposition of R^N into subspaces U and V is such that U contains $\mathrm{Ker}\,\mathbf{P}$, that is, the associated affine subspace should be tangent to the local constraint surfaces. This offers a wide range of possibilities and this report aims at examining choices alternate to the original definition.

In the original splitting method, e.g. in [2] [5], the orthogonal decomposition was based on the diagonalization of the following "reduced Hessian"

$$\mathbf{H}'_A = \mathbf{P}\mathbf{H}^+_A\mathbf{P}. \tag{22}$$

The eigenvectors of this matrix form a specific orthogonal basis made of the basis of $\mathrm{Ker}\,\mathbf{P}$, $\{q^k\}$ $(k = 1, \ldots, K)$, augmented of some other orthogonal vectors, say $\{q^k\}$ $(k = K+1, \ldots, N)$. Define the matrix

$$\mathbf{Q}' = \Big([q^{K+1}][q^{K+2}]\cdots[q^N]\Big). \tag{23}$$

Thus the original choice of splitting only accounted for the cost functions of Group A, considered preponderant, and the linearized constraints via matrix $\mathbf{P}$. Presently, we aim to devise alternate splittings to account for a balance between the directions of main influence of both Groups A and B via their Hessians.

Various splittings can be constructed by completing differently the orthonormal basis of $\mathrm{Ker}\,\mathbf{P}$ made of the vectors $\{q^k\}$ $(k = 1, \ldots, K)$. For this, consider the generalized eigenproblem

$$\big(|\mathbf{H}_B| - \lambda\mathbf{H}^+_A\big)\mathbf{x} = 0 \tag{24}$$

in which $\mathbf{H}^+_A$ and $\mathbf{H}_B$ are real-symmetric matrices evaluated at the starting point $\mathbf{x}^\star_A$, and $\mathbf{H}^+_A$ is positive-definite since the primary steering function $f^+_A(\mathbf{x})$ is constructed to be locally convex. Recall that if the diagonalization of the matrix $\mathbf{H}_B$ writes $\mathbf{H}_B = \Omega_B\Lambda_B\Omega^t_B$, where Ω_B is orthogonal and Λ_B diagonal, the "absolute value matrix $|\mathbf{H}_B|$ writes $|\mathbf{H}_B| = \Omega_B|\Lambda_B|\Omega^t_B$, and evidently it is positive semi-definite.

One may question whether it is appropriate to introduce the absolute-value matrix $|\mathbf{H}_B|$ and not the matrix $\mathbf{H}_B$ itself in the above generalized eigenproblem. The alternate choice will be demonstrated to be disastrous by our numerical experiments.

We aim to solve the generalized eigenproblem in the $(N-K)$-dimensional subspace orthogonal to $\mathrm{Ker}\,\mathbf{P}$. The calculations are performed using the column-vectors of matrix $\mathbf{Q}'$ as a basis of this subspace. Thus, let $\mathbf{x} = \mathbf{Q}'\mathbf{y}$ in which $\mathbf{y} \in \mathsf{R}^{N-K}$ in (24), and get:

$$(\mathbf{Q}')^t\big(|\mathbf{H}_B| - \lambda\mathbf{H}^+_A\big)\mathbf{Q}'\mathbf{y} = 0. \tag{25}$$

Technically we solve the above generalized eigenproblem by the Lapack procedure DSYGV which provides the generalized eigenvalues $\{\lambda^j\}$ $(j = 1, \ldots, N-K)$, which are all positive, and the associated generalized eigenvectors $\{\mathbf{y}^j\}$ $(\mathbf{y}^j \in \mathsf{R}^{N-K})$.

Let $\overline{\mathbf{H}}_B = (\mathbf{Q}')^t|\mathbf{H}_B|\mathbf{Q}' = \Theta_B|\Lambda_B|\Theta^t_B$, in which the $(N-K)\times N$ matrix $\Theta_B = (\mathbf{Q}')^t\Omega_B$ is such that $\Theta_B\Theta^t_B = (\mathbf{Q}')^t\mathbf{Q}' = \mathbf{I}_{N-K}$ since Ω_B is orthogonal, and the column-vectors of matrix $\mathbf{Q}'$ have been generated by the Gram-Schmidt process, and are thus orthonormal. The matrix $\overline{\mathbf{H}}_B$ represents the restriction of the endomorphism represented by $|\mathbf{H}_B|$ to the subspace $\mathrm{Ker}\,\mathbf{P}^\perp$. In general, this matrix is not scalar, and the generalized eigenvectors known to be $\overline{\mathbf{H}}_B$-orthogonal, form a complete basis of R^{N-K}, since the eigenproblem is symmetric, but this basis is not orthogonal.

Five different alternate splittings, designated AS1 to AS5, have been defined and tested numerically. The first two correspond to the following choices:

1. AS1: to privilege subspace U, a basis of it is defined by supplementing the basis of $\mathrm{Ker}\,\mathbf{P}$ made of $\{\mathbf{q}^1, \ldots, \mathbf{q}^K\}$ with the generalized eigenvectors associated with the $N-K-p$ smaller generalized eigenvalues;

2. AS2: to privilege subspace V, a basis of it is defined as the set of the generalized eigenvectors associated with the p larger generalized eigenvalues.

The rationale is as follows:

- For very large λ, or $|\mathbf{H}_B|$ scalar, AS1 identifies to the original splitting; hence we see the strategy in AS1 as privileging the effort to maintain at best the quasi Pareto-stationarity of the primary cost functions.
- Inversely, AS2 is expected to privilege the reduction of the secondary cost functions, perhaps at the cost of a larger departure from the Pareto-stationarity of the primary cost functions.

For the sake of completeness, the following counter-intuitive splittings have also been evaluated experimentally:

3. AS3: a basis of subspace U is defined by supplementing the basis of $\mathrm{Ker}\,\mathbf{P}$ made of $\{\mathbf{q}^1, \ldots, \mathbf{q}^K\}$ with the generalized eigenvectors associated with the $N-K-p$ *larger* generalized eigenvalues;
4. AS4: a basis of subspace V is defined to be made of the generalized eigenvectors associated with the p *smaller* generalized eigenvalues;
5. AS5: no privilege: $N-K$ vectors of dimension $N-K$ chosen by random draw.

Once made the choice of privileging Subspace U (resp. V), and correspondingly $N-K-p$ (resp. p) generalized eigenvectors of a kind, according to one of the above alternate splittings, these basis vectors are placed first in a list that is then completed either with the p (resp. $N-K-p$) tail column-vectors of matrix $\mathbf{Q}'$ to form a complete basis of R^{N-K}. Then, the Gram-Schmidt process is applied to this basis, resulting in two effects:

– it transforms the basis of the privileged subspace into an orthonormal basis of it;

– it completes the cited-above basis with orthogonal vectors; the latter ones span the subspace supplementary to the privileged one; this supplementary subspace is not, in general, the subspace spanned by the discarded generalized eigenvectors since the generalized eigenvectors are $\overline{\mathbf{H}}_B$-orthogonal, that is, *not orthogonal*.

The vectors are then expressed in the canonical basis using matrix $\mathbf{Q}'$ ($\mathbf{x} = \mathbf{Q}'\mathbf{y}$). Lastly, the resulting N-vectors are allocated accordingly to either complete the basis of Subspace U (in addition to the basis of $\mathrm{Ker}\,\mathbf{P}$), or to define a basis of Subspace V.

Matrix $\mathbf{\Omega}$. The complete orthogonal basis is stored in an $N \times N$ matrix $\mathbf{\Omega}$, split into the $N \times (N-p)$ left block, denoted $\mathbf{\Omega_u}$, whosr range spans U, and the $N \times p$ right block, denoted $\mathbf{\Omega_v}$, whose range spans V. This completes the construction of Section 3.

Implementation. The basic computer program is modified to include an additional logical parameter "*nsplit*" equal to 0 for the original splitting, and from 1 to 5 for the alternate splittings. With $nsplit = 0$, various data calculated in the preparation of the Nash games are written on a dedicated file (starting point $\mathbf{x}_A^\star$, values of cost functions and their approximate gradients, $\mathbf{Q}$ matrix, convexity-fix constant c). Then, a separate program uses this information to calculate the matrices $\mathbf{\Omega_u}$ and $\mathbf{\Omega_v}$ for the different splittings. Finally, when executing the code with $nsplit \neq 0$, these definitions are used in place of the diagonalization of matrix $\mathbf{H}_A^+$.

6.2 Numerical experiments on the sandwich panel test-case

The test-case of Subsection 5.2 was again considered to compare the various proposed splittings. Note that the following experiments have been conducted using the same values of the numerical parameters as those used in Subsection 5.2; those had been roughly optimized. This may have given some advantage to the classical method over the variants, in particular w.r.t. the convexity-fix constant. This possible effect has not been assessed.

Unscaled functions. By solving the generalized eigenproblem (25), the generalized eigenvalues were found to be:

$$\Lambda = (0.725772, 6.094200, 27.249456, 37.819957) \tag{26}$$

all *strictly*-positive. The corresponding condition number of Λ is close to 52.1. The generalized eigenvectors have been normalized and formed the following matrix:

$$\mathbf{Y} = \begin{pmatrix} -0.001943 & 0.998686 & 0.045607 & 0.002052 \\ -0.000038 & 0.001013 & 0.020936 & -0.999733 \\ -0.000049 & 0.051092 & -0.998740 & -0.023027 \\ 0.999998 & 0.003884 & 0.000092 & -0.000068 \end{pmatrix} \tag{27}$$

Figure 5 provides the variation of the cost functions with $\varepsilon/\varepsilon_{\max}$ for the original splitting (a), and the five alternate ones (b through f). On each plot, the value of $\varepsilon_{\max}$ is indicated above the horizontal axis.

Firstly, we observe that AS1 and AS2 on one side, and AS3 and A4 on the other side yield almost the same result. This is because the generalized eigenvectors are almost orthogonal, as it is revealed by the matrix

$$\mathbf{I} - \mathbf{Y}^t\mathbf{Y} = \begin{pmatrix} 0.000000 & -0.194111 & -0.005117 & 0.003352 \\ -0.194111 & 0.000000 & 0.545951 & 0.014050 \\ -0.005117 & 0.545951 & 0.000000 & -0.216156 \\ 0.003352 & 0.014050 & -0.216156 & -0.000000 \end{pmatrix}_{\times 10^{-2}} \tag{28}$$

in which the numerical entries are expressed as multiples of 10^{-2}. Hence the discrepancy with orthogonality is hardly visible at the scale of the figure.

Secondly, compared with the original splitting (a), AS1 (b), or equivalently AS2 (c), has its own merit. The initial slope of the secondary steering function is notably greater in absolute value. The secondary cost function f_4 is more importantly reduced, and the decay of the two secondary cos functions is remarkably similar, and initially very close to their steering function. These benefits are realized at the cost of a superior degradation of the Pareto-optimality of the primary cost functions, illustrated by the greater rate of increase of f_1 (mass), while f_2 remains close to constant.

Thirdly, unsurprisingly, the counter-intuitive assignment of generalized eigenvectors to span the subspaces U and V leads to totally ineffective algorihms. Still, in a sense, the Nash equilibria are observed to respect trivially the theory, by maintaining all the normalized functions to 1 until the process blows up at the very end, very close to the limit of convexity.

Lastly, AS5 does almost as well w.r.t. f_1, f_3 and f_4, but here f_2 increases, and this is a degradation of the result.

Rescaled functions. The experiment is repeated using this time the rescaled functions $\{\tilde{f}_j(\mathbf{x})\}$.

By solving the new generalized eigenproblem (25), the generalized eigenvalues were found to be:

$$\Lambda = (0.773283, 5.818311, 11.446667, 12.756895) \tag{29}$$

again all *strictly*-positive. The corresponding condition number of Λ is now reduced to 16.5 which indicates that the new system is better conditioned. The generalized eigenvectors have been normalized and formed the following matrix:

$$\mathbf{Y} = \begin{pmatrix} 0.008014 & 0.642729 & 0.748062 & -0.109221 \\ -0.006376 & -0.763822 & 0.628491 & -0.155664 \\ -0.000274 & 0.055653 & -0.213036 & -0.981753 \\ 0.999948 & -0.019433 & -0.004146 & -0.000640 \end{pmatrix} \tag{30}$$

The corresponding results are given in Figure 6 .

With the original splitting (a), the variations are smaller, but the scale on the vertical axis has changed. The graphs of two primary cost functions are close to be symmetrical, which indicates a greater vicinity to the PPF. A small but visible reduction of $\tilde{f}_2$ is now visible. Hence rescaling resulted in a qualitatively better configuration of the funnel-shape pattern.

Again, AS1 and AS2 are almost equivalent, since the matrix

$$\mathbf{I} - \mathbf{Y}^t\mathbf{Y} = \begin{pmatrix} -0.000000 & 0.094265 & 0.020994 & 0.002539 \\ 0.094265 & 0.000000 & 0.110300 & 0.059248 \\ 0.020994 & 0.110300 & 0.000000 & -0.296143 \\ 0.002539 & 0.059248 & -0.296143 & 0.000000 \end{pmatrix}_{\times 10^{-1}} \tag{31}$$

has small entries, although somewhat larger in magnitude compared with the unscaled case of (28).

Again, AS3 and AS34 are totally ineffective.

Again, AS5 based on random draws performs amazingly well since it permits a significant reduction of $\tilde{f}_2$. Since the variations of $\tilde{f}_2$ and $\tilde{f}_3$ from 1 are close to opposite, while the convex coefficients defining the primary steering function are both very close to $\frac{1}{2}$, the Pareto-stationarity condition is only weakly degraded. Both secondary cost functions have a very similar decay, corresponding to a large reduction at the final stage. This result is therefore fairly satisfactory.

To confirm these observations, the same data have been expressed in terms of the original cost functions, and corrrespondingly plotted in Figure (7). For purpose of a quantitative comparison, the plots have here been cut at $f_1 = 1.1$ which corresponds to a tolerated 10% mass increase.

AS1, or equivalently AS2, results in a slightly inferior reduction of f_3, but with the benefit of a superior, nearly equivalent reduction of f_4.

AS3 and AS4 are unacceptable.

With AS5, the reduction of f_3 is inferior, but the general pattern is in nice conformity with the theoretical expectation.

An experiment with a different generalized eigenvalue problem. One may question whether the use of matrix $\mathbf{H}_B$ itself instead of $|\mathbf{H}_B|$ in the generalized eigenproblem (24) and (25) could be appropriate. After doing this substitution in the generalized eigenproblem (25), the generalized eigenvalues were newly found to be:

$$\Lambda = (-37.819315, -27.244426, 0.725772, 6.094302) \tag{32}$$

that is, two were strictly-negative and two strictly-positive. The corresponding condition number of $|\Lambda|$ is close to 52.2. Their set of absolute values is close to, but slightly different from the set of generalized eigenvalues in (26). Here, the normalized generalized eigenvector matrix was found to be:

$$\mathbf{Y} = \begin{pmatrix} -0.002108 & 0.048266 & -0.001943 & -0.998529 \\ 0.999729 & 0.021092 & -0.000037 & -0.000999 \\ 0.023194 & -0.998612 & -0.000050 & -0.054068 \\ 0.000067 & 0.000099 & 0.999998 & -0.003884 \end{pmatrix} \tag{33}$$

In spite of small numerical discrepancies, the similarity of (32)-(33) with (26)-(30) after appropriate permutations of eigenvalues and correspondingly eigenvector-matrix column-vectors is evident. Clearly, the pair of the above eigenvectors associated with the algebraically smaller (resp. larger) two eigenvalues is almost the same as the pair formerly associated with the larger (resp. smaller) two. Hence this new partition would essentially transform the definition of AS1 (resp. AS2) into AS3 (resp. AS4), and result in an inversion of the roles of U and V.

This is confirmed by Figure 8 which provides the variation of the cost functions for the original splitting (a), and the five alternate ones (b through f). Unsurprisingly, we observe almost equivalent results as in Figure 5) after permutation.

Hence this option results in counter-intuitive trends, and it is abandoned.

Final recommendation. Let $(\mathbf{y}, \lambda)$ be an associated solution pair of the generalized eigenproblem (25) so that:

$$(\mathbf{Q}')^t|\mathbf{H}_B|\mathbf{Q}'\mathbf{y} = \lambda(\mathbf{Q}')^t\mathbf{H}_A^+\mathbf{Q}'\mathbf{y}. \tag{34}$$

Evidently

$$\lambda^2(\mathbf{Q}')^t\left(\mathbf{H}_A^+\right)^2\mathbf{Q}'\mathbf{y} = \lambda^2(\mathbf{Q}')^t|\mathbf{H}_B|\underbrace{\mathbf{Q}'(\mathbf{Q}')^t}_{\mathbf{I}_N}|\mathbf{H}_B|\mathbf{Q}'\mathbf{y} = \lambda^2(\mathbf{Q}')^t\mathbf{H}_B^2\mathbf{Q}'\mathbf{y}. \tag{35}$$

Unsurprisingly, $(\mathbf{y}, \lambda^2)$ is an associated solution pair of the generalized eigenproblem obtained by replacing the matrices $\mathbf{H}_A^+$ and $\mathbf{H}_B$ by their respective squares in (25). Thus, by this replacement, the resulting generalized eigenvectors are the same, and the corresponding eigenvalues are the squares of the original ones, that were positive and consequently ordered in the same way. This alternate formulation is recommended since it avoids the synthesis of the matrix $|\mathbf{H}_B|$ which necessitates a diagonalization.

7 Summary, conclusions and perspectives

We firstly recalled the main aspects of the prioritized multiobjective optimization technique which develops in two phases. The first optimization phase only involves a so-called primary set of cost functions and it results in the establishment of a Primary Pareto Front (PPF). The technical realization of the first phase was not discussed here, but the assumption was implicitly made that it would become of greater difficulty with a larger number of primary cost functions, either in terms of computational cost, or logical complexity, often both. In the second optimization phase, a continuum of Nash equilibria originating from a point $\mathbf{x}_A^\star$ of the Primary Pareto Set is calculated economically yielding quasi Pareto-optimal solutions w.r.t. an enhanced set of objective functions, including both primary and secondary cost functions. These solutions realize a trade-off between the least degradation of the Pareto-stationarity of the primary cost functions, and the most effective reduction of the secondary cost functions in the neighborhood of the PPF. The Nash games are virtual; they involve two concurrent players whose respective strategies are chosen to lie in supplementary subspaces U and V of the design space. This decomposition was referred to as a "territory splitting". In this report, we began by showing that the sole condition under which the method converges was that the splitting should be such that U be tangent to the local constraint surfaces. This result has generalized somehow the detailed proof given in [5].

This generalization has encouraged us to examine various forms of territory splitting respecting the above convergence condition. Several possible choices have been defined from the structure of the solution of a generalized eigenvalue problem realizing a balance between primary and secondary cost functions via their approximate Hessians.

The different splittings have been tested numerically in a case of optimum sizing of an aluminum sandwich panel subject to flexural forces or a blast. The physical setting was already introduced in a previous report [7]. However, the optimization test-case here has been slightly modified from the previous work, but still involving two primary cost functions, two secondary, one functional constraint, and five variables.

In particular, two splittings designated AS1 and AS2 were devised to privilege the construction of either subspace U or V. They were found equivalent in the numerical experiments because the generalized eigenvectors were found to be almost orthogonal. We expect that in a problem involving a larger number of variables, assigned unevenly to U and V, AS1 and AS2 would likely be better distinguished.

A simple rescaling procedure of the cost functions was also proposed, devised to make the values of the rescaled cost functions and the norms of their gradients initially equal to 1.

Compared with the original method, AS1, or AS2, was found to better equilibrate the decay of the two secondary cost functions. Rescaling also had this favorable effect, yielding a better-conditioned optimization system. However, this was at the cost of a more rapid degradation of the Pareto-stationarity of the primary cost functions, however less serious when using rescaling. The present scaling procedure was mostly efficient on the secondary cost functions; perhaps another rescaling principle would be more effective on the primary cost functions.

In conclusion, this report has brought some light on the question of the choice of territory splitting, but the question still remains open since other constructions could be envisaged and the optimal solution should likely depend on the problem and the designer's biases.

(a) Original Splitting (data of Fig. 3a)

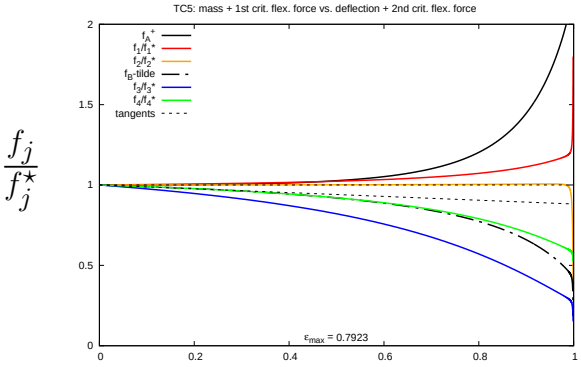

(b) AS1

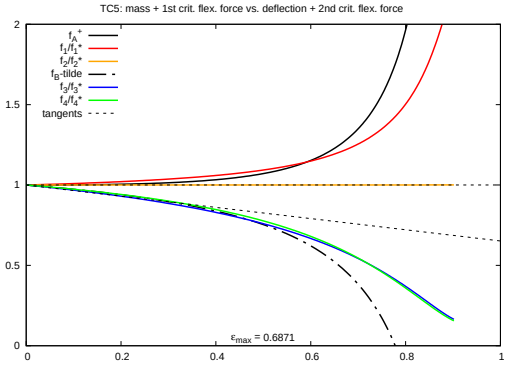

(c) AS2

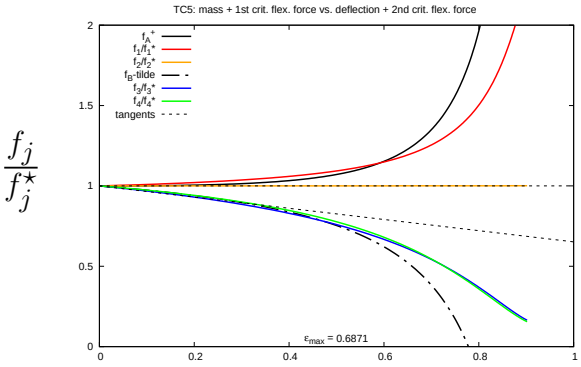

(d) AS3

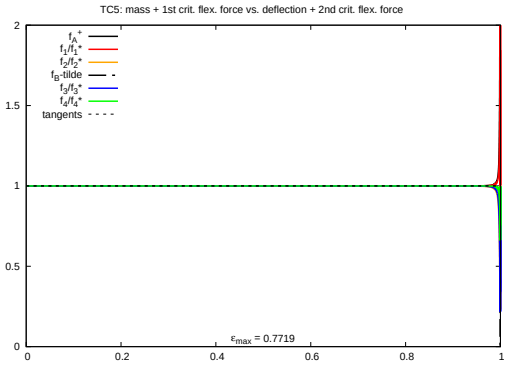

(e) AS4

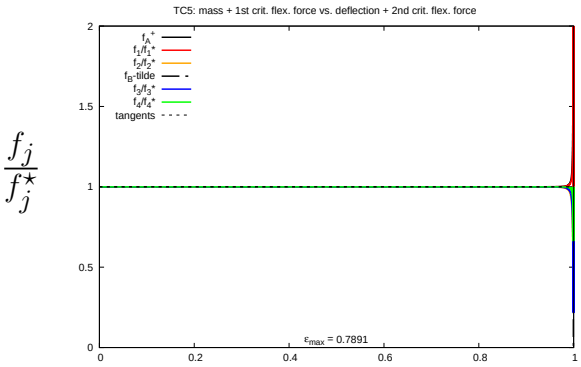

(f) AS5

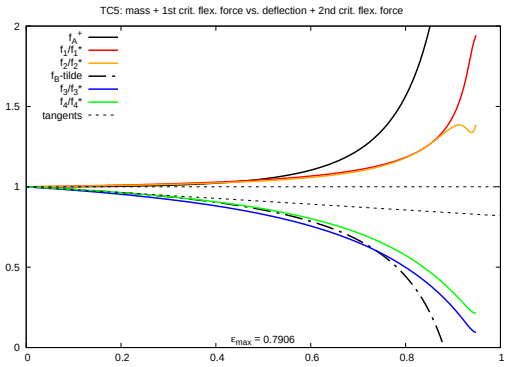

$\frac{f_j}{f_j^\star}$

$\frac{\varepsilon}{\varepsilon_{\max}}$

Figure 5: Variation of the four normalized cost functions $f_j/f_j^\star$ in terms of $\varepsilon/\varepsilon_{\max}$ along the continuum of Nash equilibria for the six considered splittings

(a) Original Splitting (data of Fig. 4a) (b) AS1

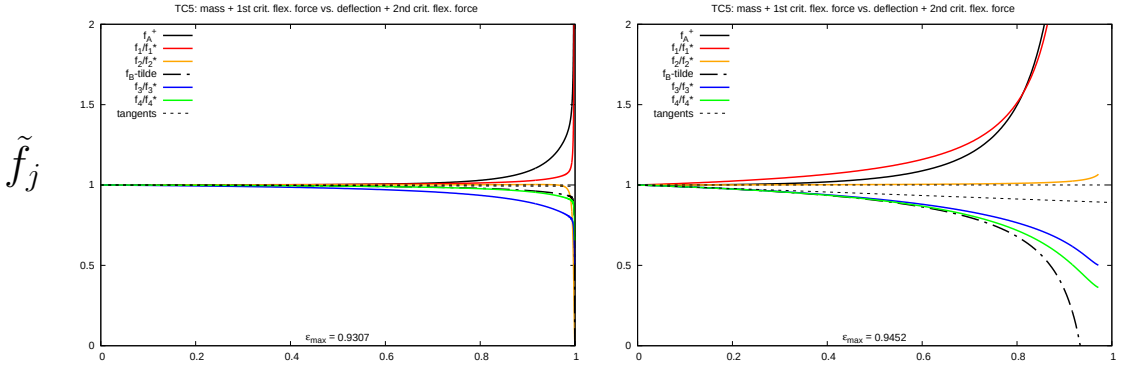

(c) AS2) (d) AS3

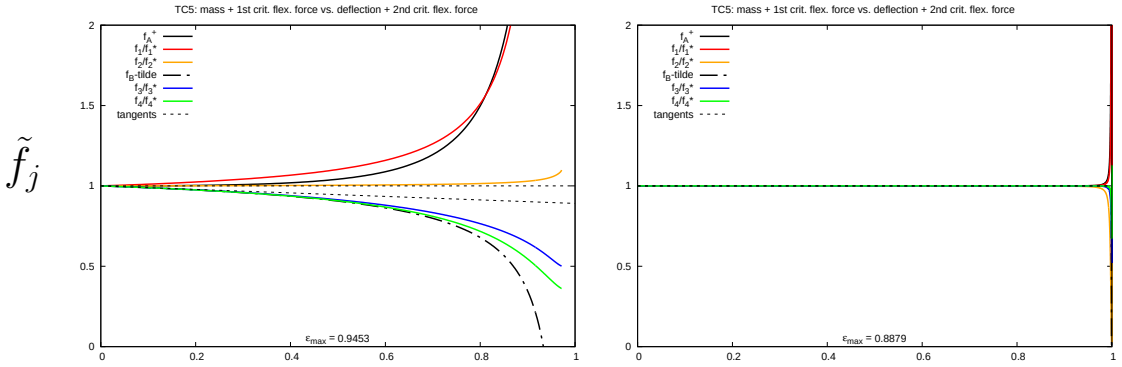

(e) AS4 (f) AS5

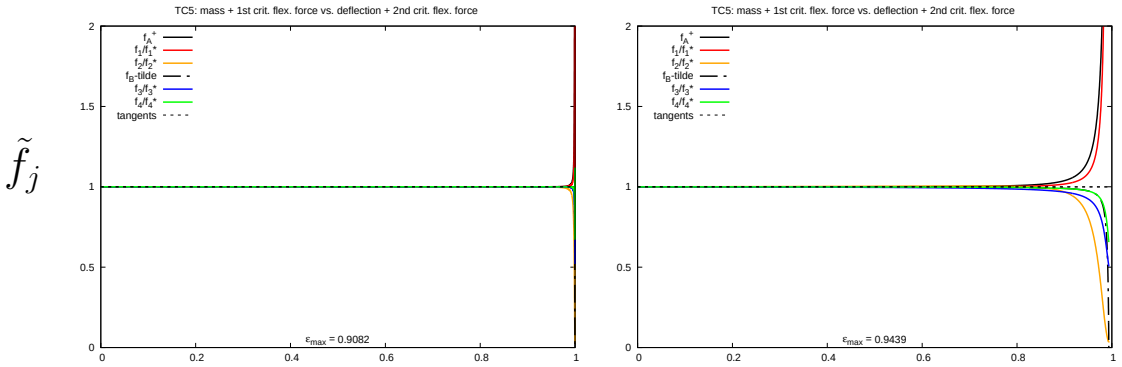

$\tilde{f}_j$

$\frac{\varepsilon}{\varepsilon_{\max}}$ $\frac{\varepsilon}{\varepsilon_{\max}}$

Figure 6: Variation of the four rescaled cost functions $\tilde{f}_j$ in terms of $\varepsilon/\varepsilon_{\max}$ along the continuum of Nash equilibria for the six considered splittings

(a) Original Splitting (data of Fig. 6a)

(b) AS1 (data of Fig. 6b)

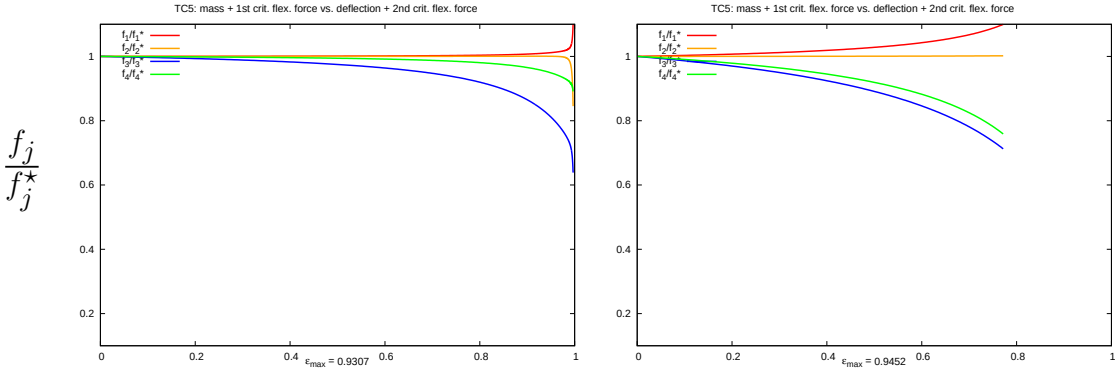

(c) AS2 (data of Fig. 6c)

(d) AS3 (data of Fig. 6d)

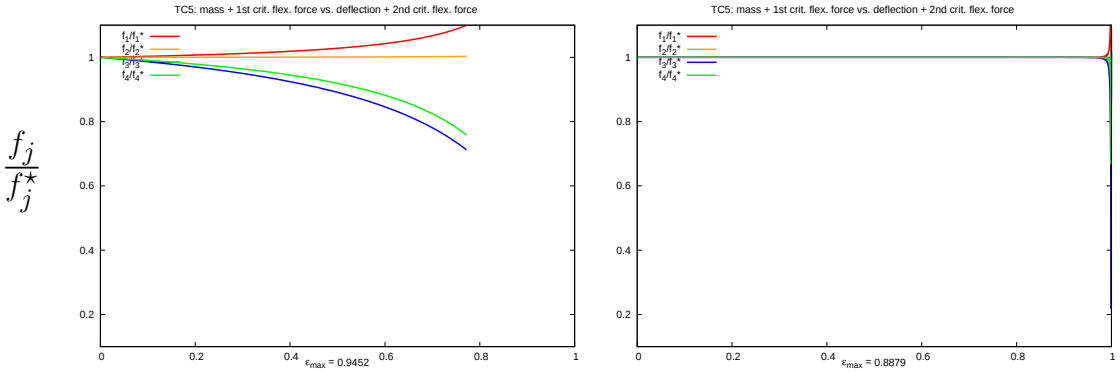

(e) AS4 (data of Fig. 6e)

(f) AS5 (data of Fig. 6f)

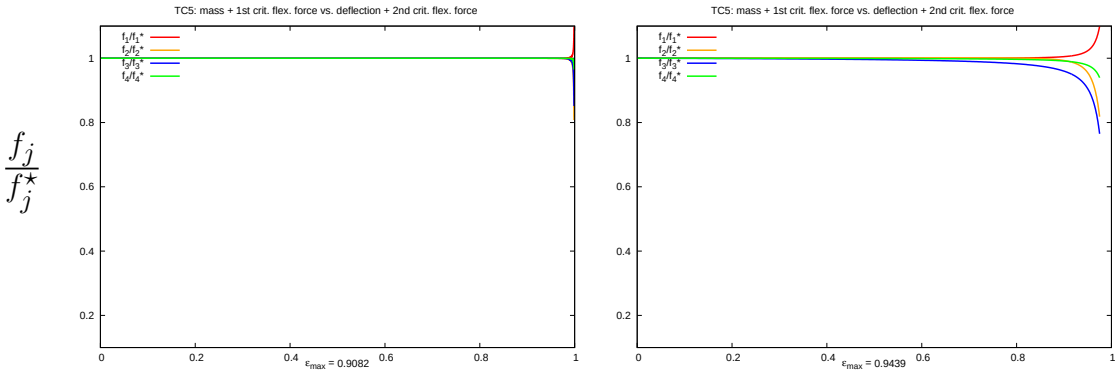

$\frac{f_j}{f_j^\star}$

$\frac{\varepsilon}{\varepsilon_{\max}}$

Figure 7: Variation of the four original (unscaled) cost functions f_j in terms of $\varepsilon/\varepsilon_{\max}$ along the continuum of Nash equilibria for the data of Figure 6

(a) Original Splitting (data of Fig. 3a)

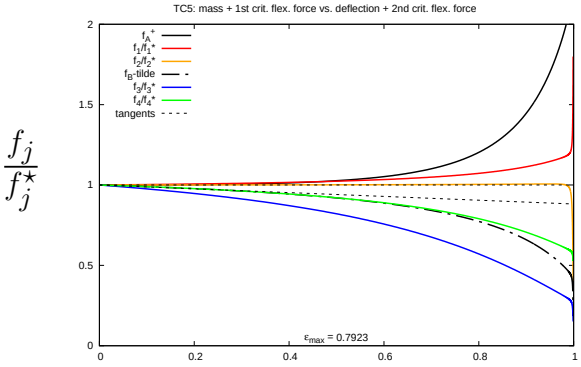

(b) AS1

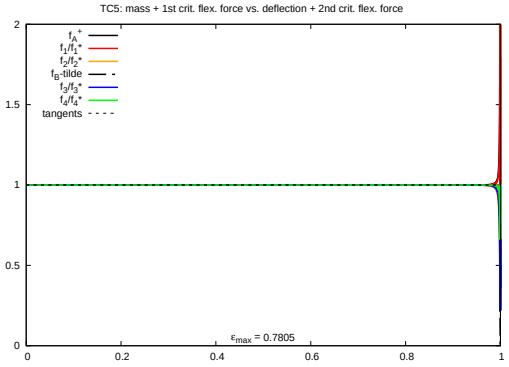

(c) AS2

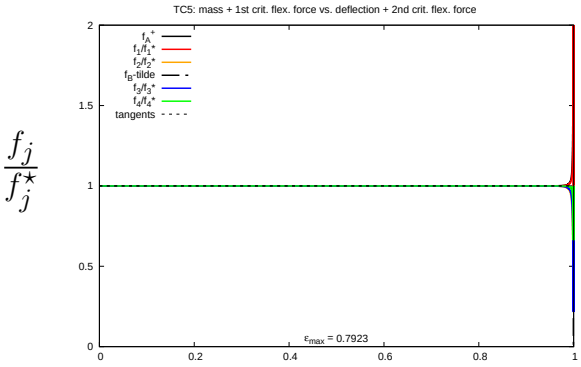

(d) AS3

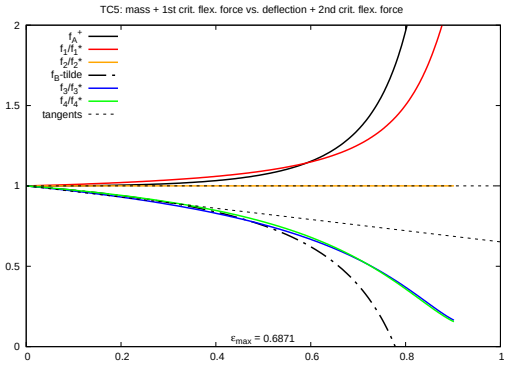

(e) AS4

(f) AS5

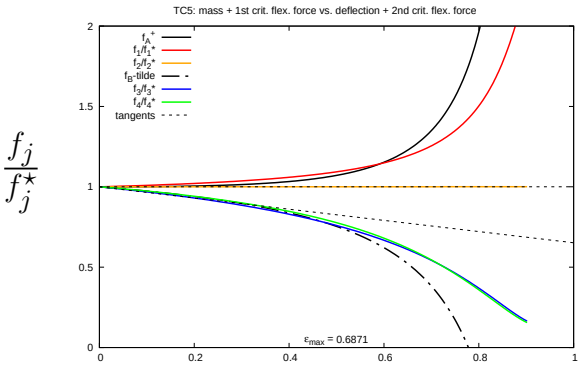

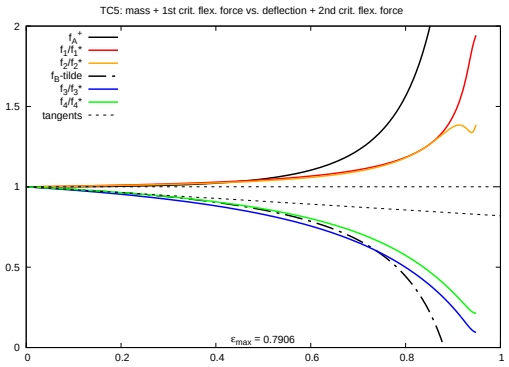

$\frac{f_j}{f_j^\star}$ $\frac{\varepsilon}{\varepsilon_{\max}}$ $\frac{\varepsilon}{\varepsilon_{\max}}$

Figure 8: Variation of the four normalized cost functions $f_j/f_j^\star$ in terms of $\varepsilon/\varepsilon_{\max}$ along the continuum of Nash equilibria for the six considered splittings

References

[1] K. Deb, A. Pratap, S. Agarwal, and T. Meyarivan, *A fast and elitist multiobjective genetic algorithm: NSGA-II*, IEEE Transactions on Evolutionary Computation, 6 (2002), pp. 182–197.

[2] J.-A. Désidéri, *Optimisation Multidisciplinaire en Mécanique 1: démarche de conception, stratégies collaboratives et concourantes, multiniveau de modèles et de paramètres, Rajan Filomeno Coelho, Piotr Breitkopf eds.*, Hermes Science Publications-Lavoisier, 2009, ch. 5: Partage de territoire en ingénierie concourante.

[3] ——, *Quasi-Riemannian multiple gradient descent algorithm for constrained multiobjective differential optimization*, Research Report 9159, Inria, 21 March 2018. `https://hal.inria.fr/hal-01740075v1`.

[4] ——, *Platform for prioritized multi-objective optimization by metamodel-assisted Nash games*, Research Report 9290, Inria, September 2019. `https://hal.inria.fr/hal-02285197`.

[5] ——, *Adaptation by Nash games in gradient-based multi-objective/multi-disciplinary optimization*, in JANO13, Mathematical Control and Numerical Applications, Khouribga, Morocco, vol. 372, Springer Proceedings in Mathematics and Statistics, 2021. `https://hal.inria.fr/hal-03430972`.

[6] J.-A. Désidéri and R. Duvigneau, *Prioritized optimization by Nash games: towards an adaptive multi-objective strategy*, in ESAIM: Proceedings and Surveys, vol. 71, EDP Sciences, 2021, pp. 54–63. `https://hal.inria.fr/hal-03430912`.

[7] J.-A. Désidéri, P. Leite, and Q. Mercier, *Prioritized multi-objective optimization of a sandwich panel*, Research Report 9362, Inria, September 2020. `https://hal.inria.fr/hal-02931770`.

[8] J.-A. Désidéri, J. Wintz, N. Bartoli, C. David, and S. Defoort, *Combining Pareto Optimality with Nash Games in Multi-Objective Prioritized Optimization of an Aircraft Flight Performance*, Research Report RR-9490, Inria - Sophia Antipolis ; Acumes, Oct. 2022.

[9] J.-A. Désidéri, J. Wintz, M. Binois, N. Bartoli, C. David, and S. Defoort, *Prioritized multi-objective optimization of an aircraft flight performance based on Nash games from preponderant Pareto-optimal points.* working paper or preprint, Dec. 2024.

[10] M. Emmerich, K. Yang, A. Deutz, H. Wang, and C. M. Fonseca, *Advances in Stochastic and Deterministic Global Optimization, P. M. Pardalos and A. Zhigljavsky and J. Žilinskas eds.*, Springer Optimization and Its Applications, Springer, Cham, 2016, ch. A Multicriteria Generalization of Bayesian Global Optimization.

RESEARCH CENTRE
Centre Inria d'Université Côte d'Azur

2004 route des Lucioles - BP 93
06902 Sophia Antipolis Cedex

Publisher
Inria
Domaine de Voluceau - Rocquencourt
BP 105 - 78153 Le Chesnay Cedex
inria.fr

ISSN 0249-6399